A&A manuscript no.
(will be inserted by hand later)

Your thesaurus codes are:
08.06.2; 08.16.5; 08.09.2:HD 97300; 08.03.4; 13.09.4

ASTRONOMY
AND
ASTROPHYSICS
July 1, 1998

A ring of organic molecules around HD 97300*

R. Siebenmorgen[1], A. Natta[2], E. Krügel[3], T. Prusti[1]

[1] ISO Science Operations Centre, Astrophysics Division of ESA, Villafranca del Castillo, P.O. Box 50727, E-28080 Madrid
[2] Osservatorio Astrofisico di Arcetri, Largo E. Fermi 5, I-50125 Firenze
[3] MPIfR, Auf dem Hügel, D-5300 Bonn

Received .....; accepted ......

Abstract. This paper presents spectro-photometric images of the pre–main–sequence Herbig AeBe star HD 97300 in the mid-IR obtained with ISOCAM on board of ISO. The images show extended emission, an elliptical ring structure of size about $0.045{\times}0.03$ pc as well as two peaks of emission, separated by about $3''$ (240 AU). One of the two peaks coincides with the position of HD 97300, while the other may be an embedded companion. The data show that the emission in this region is dominated by the infrared emission bands centered at 6.2, 7.7, 8.7, 11.3 and 12.5 μm, with a very small contribution from continuum emission at longer wavelengths. We fit the spectra with a dust model including organic molecules such as polycyclic aromatic hydrocarbons, very small graphite and very small silicates, as well as large grains. The fit to the ISOCAM data is very good if one applies a classical oscillator model for the infrared emission bands. Our fitting procedure allows us to estimate the total mass of the ring, which is $\sim$0.03M$_\odot$. Its possible origin is briefly discussed.

Key words: star formation, Herbig AeBe stars, dust bands

1. Introduction

We present the results of imaging spectroscopy of the pre-main–sequence star HD 97300, obtained with the infrared camera (ISOCAM, Cesarsky et al. 1996a) and circular variable filter wheel on board of the infrared space observatory (ISO, Kessler et al., 1996). The data presented here are the first results of a program aimed at investigating the nature of the mid-infrared emission associated to Herbig AeBe stars. The young star HD 97300 is located in the Chamalion I cloud (Whittet et al. 1997), at distance $D \sim 188$ pc. The star excites the prominent reflection nebulosity Ced 112. Its spectral type has been estimated to be B9 (Rydgren 1980) and its luminosity $\sim$35 L$_\odot$(van den Ancker et al., 1997). Its pre-main–sequence evolutionary status (i.e., its classification among Herbig AeBe stars, or HAeBe) is based on indirect clues, namely the association with a reflection nebulosity, the presence of an infrared excess at $\lambda \gtrsim 5$ μm, and its location on the ZAMS in the HR diagram (Whittet et al. 1997). There is no evidence of significant infrared excess at wavelengths shorter than $\sim$5 μm nor of Hα emission (Thé et al. 1986). HD 97300 is very likely a relatively old object among HAeBe stars, representative of the latest stages of the pre-main–sequence evolution.

We report the detection of an extended, ring-like structure around HD 97300, whose emission is dominated by the infrared emission bands at 6.2, 7.7, 8.7, 11.3 and 12.5 μm, (hereafter IEBs), observed in our own and other galaxies wherever neutral matter is exposed to UV radiation (see for example, the review by Allamandola et al. 1989 and the many papers presenting CVF and SWS spectra in the special issue of *Astronomy and Astrophysics* on ISO published in November 1996).

2. Observations

We obtained photometric imaging of HD 97300 on February 2nd, 1996 using the long wavelength array of ISOCAM. The morphology of the object has been studied by using multi-filter observing template (The ISOCAM Team 1996). We selected four narrow band filters: lw9 (14.0 - 16.0 μm), lw8 (10.7 - 12.0 μm), lw5 (6.5 - 7.0 μm) and lw4 (5.5 - 6.5 μm). For each filter we performed 4 $\times$ 4 micro-rasters with raster step size of $5''$. We chose a pixel size of $1.5''$ and the small field mirror. The read-out time for each exposure was 2.1s. We took 75 stabilization frames in the first filter (lw9) and 30 stabilization frames in the other three. At each raster position 25 exposures have been taken. We use gain 1 for lw9 and 2 for lw8, lw5 and lw4.

Spectrophotometric images were taken on September 24th, 1997 with the circular variable filter (CVF). We used

Send offprint requests to: rsiebenm@iso.vilspa.esa.es

* Based on observations with ISO, an ESA project with instruments funded by ESA Member States (especially the PI countries: France, Germany, the Netherlands and the United Kingdom) with the participation of ISAS and NASA.

the 3″ pixel scale, the small field mirror and performed a complete downward scan from 13.83 to 9.442 μm and from 9.535 to 5.807 μm. This gave us some overlap of the two CVF segments. At each CVF step position 20 read-outs were taken with 5.04 s read-out time at gain one (see The ISOCAM Team 1996 for more details).

The data were reduced within the CIA (v1.0)[1] environment. The basic data reduction steps are described in Siebenmorgen et al. (1997). The dark current was subtracted using the calibration dark exposure scaled by a factor which depends on the orbital position of the satellite and on the revolution number (Biviano et al., private communication). Cosmic ray hits were removed with a multi-median transform method (Starck et al. 1997a,b) and transients were corrected with the IAS model (cf. Abergel et al. 1996). Flat fielding was performed using the calibration library flats.

The narrow band images at each raster position were coadded and sky-projected to construct the final raster map, which has a pixel scale of 0.5″. For flux calibration we adopted the sensitivity given by Blommaert (1997).

After coadding the exposures in each CVF step we obtained CVF photometry using the spectral response function as given from in-orbit calibrations (Biviano et al. 1997)

3. Results

Figure 1 shows the images of HD 97300 obtained in the four CAM narrow-band filters centered at 6.0 μm (lw4), 6.8 μm (lw5), 11.3 μm (lw8) and 14.9 μm (lw9). The morphology of the object is very similar in the four filters: we can see extended emission centered on the star and an elliptical ring of size $\sim 50 \times 36''$ around it. This same morphology is also seen in the CVF images at all frequencies, with very similar characteristics.

The ring is not symmetric around the star, but is much more extended in the SE than in the NW direction. The position of the star in our images coincides with the emission peaks seen near the center in lw4 and lw5, and with the secondary peak of the emission seen in lw8, roughly at the same position. In the lw8 and lw9 filters we detect a second peak of emission, about 3″ north of the star.

Figure 2 shows CVF spectra between 5.8 and 13.8 μm in 8 positions roughly aligned along P.A. = 142.4^o. This line intersects the star, as well as the emission minimum and the ring seen in the SE direction. The location of the 8 positions is indicated in Fig. 1. In all positions, we detect strong IEBs over a weak continuum. This confirms the results of Prusti et al. (1994) who found that their mid IR multi–aperture photometry was consistent with extended emission from non-thermally heated species.

[1] CIA is a joint development by the ESA Astrophysics Division and the ISOCAM Consortium led by the ISOCAM PI, C. Cesarsky, Direction des Sciences de la Matiere, C.E.A., France. Contributing ISOCAM Consortium institutes are Service d' Astrophysique (SAp, Saclay, France) and Institute d' Astophysique Spatiale (IAS, Orsay, France)

4. Discussion

4.1. An IR companion to HD 97300?

As noted in §3, we detect a secondary peak about 3″ (240 AU) north of the optical star HD 97300. This peak of emission is visible in the lw8 (10.7–12.0 μm) and lw9 (14.0–16.0 μm) filters, but not at shorter wavelengths. On the contrary, the peak of emission at the position of HD 97300 is clearly seen in the lw4, lw5 and lw8 filters, but not in lw9. Both components are clearly seen in the lw8 image. Contamination from extended emission does not allow us to determine reliable fluxes for the two components. In the CVF images, which have poorer spatial resolution than the filter ones, the two components are not separated.

The situation is reminiscent of the case of LkHα198, where an embedded companion was found near the optical star by Lagage et al. (1993) in their ground-based 10 μm images of the region. Note that in LkHα198 most of the far-infrared emission is due to optically thin dust heated by the visible star (Butner & Natta 1995). This analogy, and the dominance of the IEBs in the region, suggest to us that also in the case of HD 97300 the embedded companion does not play a major role in the energetics of the system.

4.2. The IEBs carriers

To acquire a better understanding of the nature of the IEBs, we have fitted the spectra of Fig. 2 using the dust model of Siebenmorgen & Krügel (1992). This model computes the emission per unit mass of dust heated by radiation of known intensity and spectral distribution. The dust consists of a mixture of large grains, very small grains and organic molecules. We assume here that the molecules are polycyclic aromatic hydrocarbons (PAHs), though other band carriers have been suggested (e.g. Sakata et al. 1984, Duley 1989, Papoular et al. 1989).

Only large grains are in thermal equilibrium with the incident radiation field. PAHs and small grains show strong temperature fluctuations which are treated following Siebenmorgen et al. (1992). The radiation field is that of a star of effective temperature $T_\star$=10700 K and luminosity $L_\star$=35 $L_\odot$. We assume that the projected separation between the star and the position at which the spectrum has been measured equals the physical distance, and neglect any intervening absorption. The computed spectra are smoothed to the CVF spectral resolution.

In our model, the IEBs are due to PAHs of fixed size and structure. In reality, we expect a mixture of PAHs of different size and structure. Their average composition will depend on the environment and is thus likely to change from place to place. Nevertheless, we consider

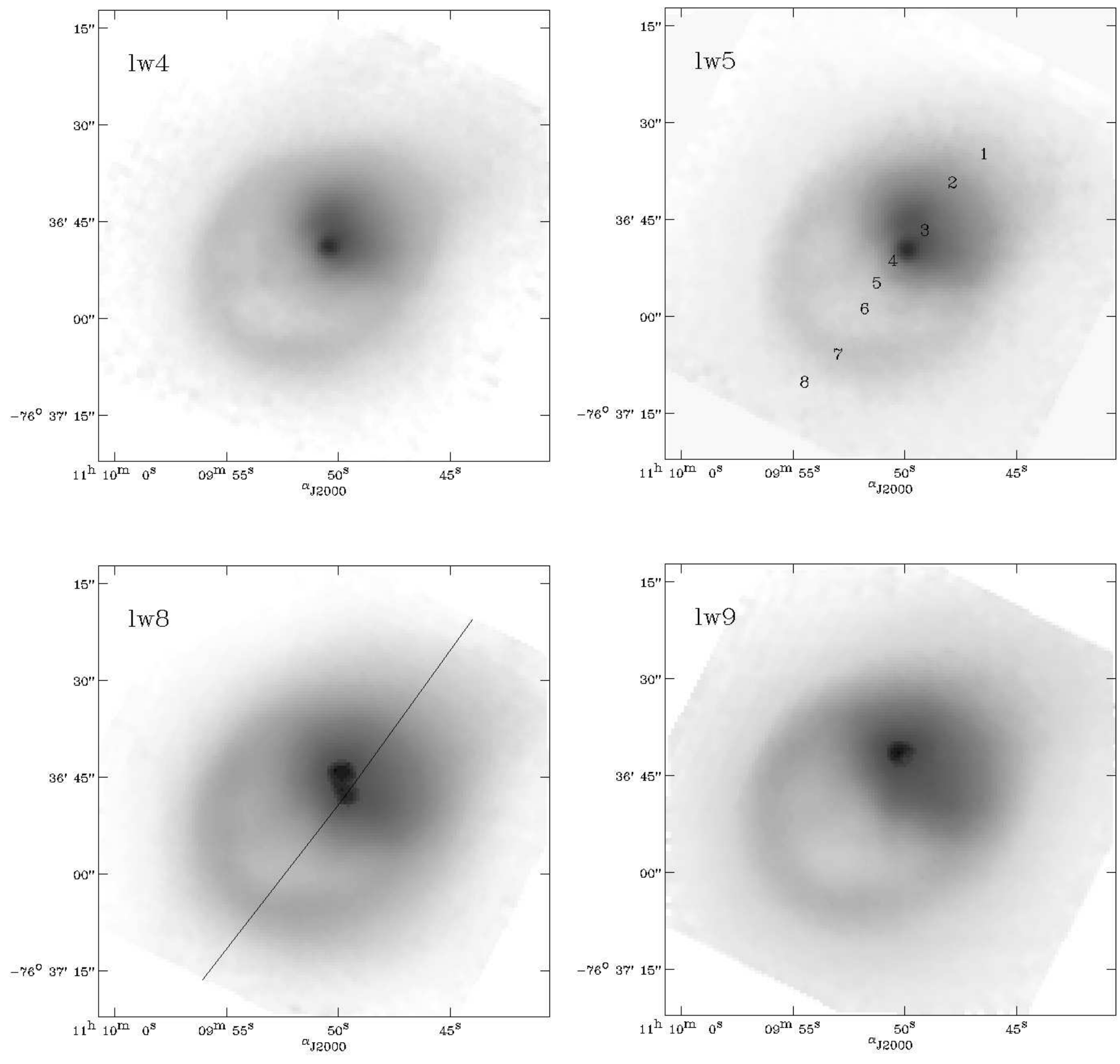

Fig. 1. Logarithmic grey scale images of HD 97300 of the four narrow-band filters. The images are re-sampled to 0.5″ pixel scale. The numbers in the lw5 image indicate the positions of the CVF spectra shown in Fig. 2. The full line in the lw8 image at P.A. $=142.4^o$ gives the direction along which the intensity profiles have been measured (see Fig. 4).

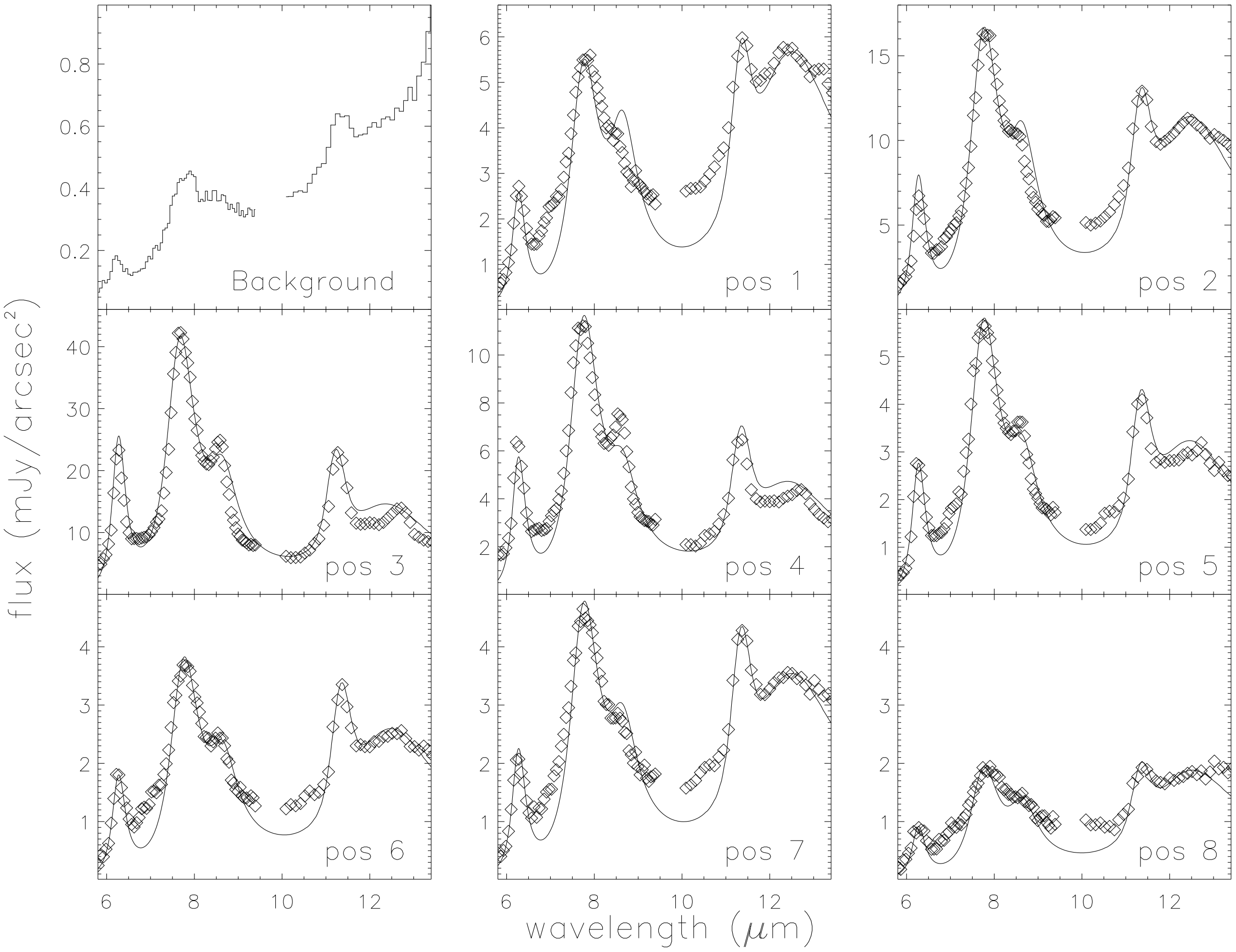

Fig. 2. CVF spectra of HD 97300 in the 8 positions shown in Fig. 1. Position 4 is closest to the star; Position 6 coincides roughly with the minimum of emission seen in the images; position 7 with the ring. The background emission has been measured in the upper-left corner of the imaged area. Each spectrum has been measured over a single pixel, i.e., over an area of $3'' \times 3''$. The uncertainties are typically smaller than a few %. Data are shown by diamonds and the best-fit models by the full lines.

for simplicity only two types of PAHs, one formed by 30 carbon atoms and one by 300. Both kinds contain 3% of the amount of carbon in large grains. In our dust model we assume a carbon abundance in solids relative to hydrogen atoms of 3 10^{-4}. The absorption cross sections of PAHs have been calculated following Schutte et al. (1993). For each IR resonance, we specify the center wavelength λ_c, the integrated cross section σ, and the shape of the line. For the latter we assume a Lorentzian profile with a damping constant γ. These numbers are listed in Table 1 and kept fixed in the calculations. For comparison, we also give the resonance cross sections of Schutte at al. (1993).

Table 1. PAH Properties

λ (Å)	$\sigma^\dagger$ (10^{-21}cm$^2\mu$m)	$\sigma^\ddagger$ (10^{-21}cm$^2\mu$m)	γ (10^{12}s^{-1})
6.3	1.8	1.8	16
7.8	4.6	12	24
8.6	6.7	6	18
11.3	17	40	5
12.5	17	19	29

† this paper
‡ Schutte et al. (1993)

For features due to C–H bonds, we additionally need the hydrogenation parameter $\alpha_{\rm H}$=[H]/[C], i.e. the ratio of hydrogen to carbon atoms in the PAH. This parameter is allowed to vary in the nebula, but is assumed to be equal for both small and large PAHs. The resonances at 11.3 and 12.5 μm are due to out–of–plane C–H bending; that at 11.3 μm is caused by isolated H atoms, while the 12.5 μm feature is caused by two adjacent H atoms. We assume that a fraction $f_{\rm H}$ of all out–of–plane C–H bending modes are due to isolated H atoms, and the rest (1-$\rm f_H$) to two adjacent ones. Also $f_{\rm H}$ may vary within the nebula.

For each position, we adjust $\alpha_{\rm H}$, $f_{\rm H}$ and the gas column density $N_{\rm H}$ until a satisfactory fit is obtained. The results are shown as solid lines in Fig. 2. Table 2 gives the position

Table 2. Model Parameters

Position	Distance (AU)	$N_{\rm H}$ ($10^{21}{\rm cm}^{-2}$)	$\alpha_{\rm H}$	$f_{\rm H}$
1	-2800	1.3	0.27	0.13
2	-1600	1.0	0.21	0.14
3	560	0.2	0.16	0.22
4	1250	0.3	0.14	0.20
5	2000	0.5	0.16	0.18
6	2800	0.7	0.18	0.18
7	4400	2.3	0.18	0.17
8	5600	1.8	0.23	0.14

in Column 1, the corresponding values of the projected distance from HD 97300 in Column 2, the gas column density ($N_{\rm H}$) in Column 3, $\alpha_{\rm H}$ in Column 4 and $f_{\rm H}$ in Column 5. The hydrogenation parameter $\alpha_{\rm H}$ is higher at larger distance from the star, while $f_{\rm H}$ decreases. This is expected (Schutte et al., 1990) since the radiation field intensity decreases as the distance from the star increases.

The agreement in Fig. 2 between model and data is generally good, considering the observational uncertainties. There are a few discrepancies, as in position 1, where the predicted intensity at 8.6μm is too strong, or in position 4, where it is too weak. Also the flux between the features is sometimes underestimated, but the peak intensities and band shapes of the resonances themselves are fitted quite well. At some places, one has a definite impression that there is a feature which is not included in the model, for example, at position 6 at 7μm.

One important characteristic of these models is the fact that, in order to obtain a good fit of the observations, we find it necessary to postulate that the features have extended wings. We model the absorption profile of each feature in a purely descriptive manner. The simplest picture we can construct is to consider that the bands can be described by classical oscillators. The absorption coefficient (σ_ν) of such a driven damped oscillator is a Lorentzian profile

$$\sigma_\nu \;=\; \frac{\sigma}{2\pi}\cdot\frac{\gamma}{(\omega-\omega_0)^2+(\gamma/2)^2}\;, \tag{1}$$

where $\omega = 2\pi\nu$. The integrated cross section σ and the damping constant γ are given in Table 1.

We are not in a position to give a physical explanation for the damping constant and restrict, therefore, their discussion to a comment. *Cum granu salis*, when in an atom an excited level has an average lifetime $t_{\rm L} = A^{-1}$, where A is the Einstein coefficient for spontaneous transition, the probability to find the atom there decays like e^{-At}. Because of Heisenberg's uncertainty principle $\Delta E\cdot\Delta t \geq \hbar$, the energy of the upper level is then only defined to an accuracy $\Delta E = A\hbar$. This leads naturally to a Lorentzian emission profile, and A may be identified with the damping constant, $\gamma = A$.

In this picture, the line width is determined by the timescale Δt. For PAH resonances with a width of $\simeq$ 0.1μm, the characteristic time Δt would be 10^{-12} s. This would imply immense values for A ($10^{12}{\rm s}^{-1}$) as well as for the associated dipole moment $\mu \sim 10^5$ Debye because $A \propto \mu^2\omega^3$. A way out of the dilemma would be to assume that the IEBs arise from a superposition of many narrow lines.

Allamandola et al. (1989) have interpreted Δt = 10^{-12} s as follows: After the absorption of a UV photon and once the PAH has arrived at the final electronic state from which it will emit the IR features, it takes about 10^{-12} s to statistically distribute the energy of the UV photon (or what is left of it) among the various vibrational levels (mostly of low vibrational quantum number, $v = 0, 1, 2$). This shuffling among the population of the levels continues while the IR photons are being emitted, so that the mean lifetime of a vibrational level is also only 10^{-12} s, which explains the observed line width.

4.3. Energetics and Continuum Emission

Our models include not only PAHs but also large grains and very small particles of carbon and silicates. We assume that the grains have a power-law size distribution ($n(a) \propto a^{-q}$) with $100 \leq a \leq 2500$Å, $q = 3.5$ for the large grains and 10$\leq a \leq 100$Å, $q = 4$ for the small particles. Small grains are 10% in mass relatively to large grains. In Fig. 3 we show the contribution of the individual dust population to the total IR emission. The spectrum is calculated for the ring (position 7). The relative contribution of the different dust species to the emitted spectrum does not depend significantly on the distance from HD 97300.

Large grains absorb 75% of the stellar radiation and emit it predominantly in the far IR. They are responsible for the IR excess observed at longer wavelengths. Given the moderate luminosity of the star the large grains are too cold to contribute to the emission observed in the spectral range of our CVF scan.

Very small grains absorb 8% of the total energy. As for PAHs, the temperature of the very small grains fluctuates violently, but the absence of any resonance smoothes out their emission over a large wavelength interval. The small grain emission peaks at about 50-60μm, and is unimportant in the range of wavelengths we have observed. However, it should be noted that the properties of very small grains are very uncertain. Their absorption cross section, computed assuming that the grains are spheres and applying the Mie theory for continuous media, is very likely underestimated. There is an enormous difference in the absorption properties between a PAH made of 300 C atoms and a very small carbon particle of the same size.

PAHs absorb about 17% of the stellar luminosity (4% is absorbed by PAH molecules and 13% by PAH clusters). They re-radiate it in the IEBs, which account for most of the emission in the CVF wavelength range.

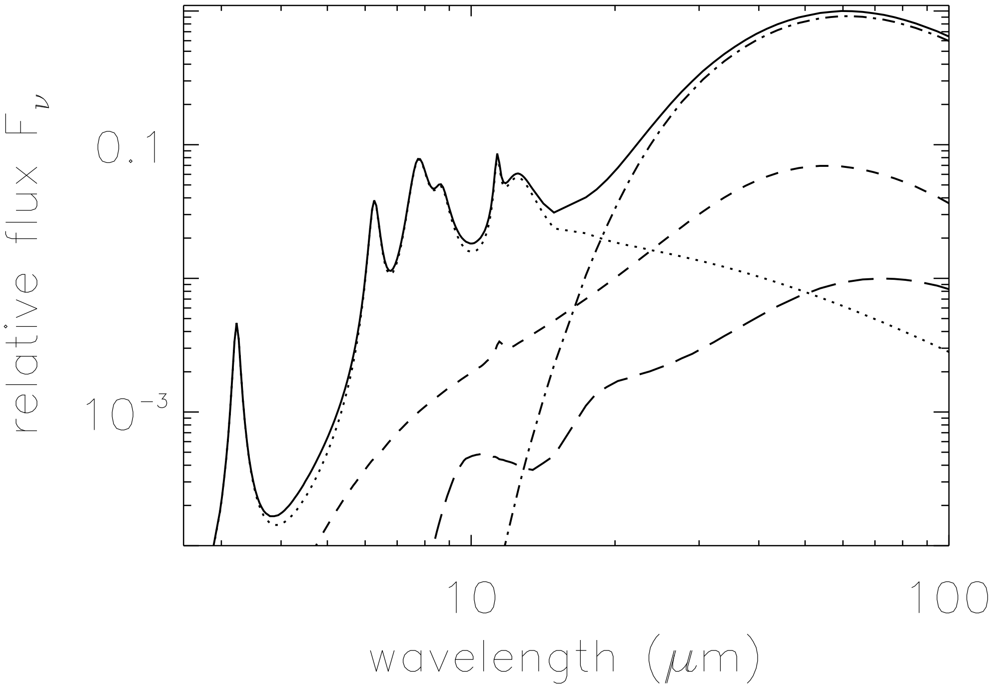

Fig. 3. Contribution of the individual dust populations to the total IR spectrum (full line). The emission of large grains is shown by the dash-dotted line, very small graphite by the dashed line, very small silicates by the long dashed line, and PAHs by the dotted line.

The CVF spectra show evidence of continuum emission at wavelengths around 7μm and in the interval 9–11μm. Continuum emission is also seen in the interval 14–16 μm. Figure 4 shows for the four narrow band filters the observed intensity as function of the distance from the star along the direction indicated in Fig. 1. The morphology of the region is very similar at all wavelengths.

The morphological similarity between the emission in the IEBs and in the continuum suggests that both are due to the same carriers, and that UV photon excitation must be the main excitation mechanism. Similar conclusions have been reached by Cesarsky et al. (1996b,c), Boulanger et al. (1996) and Uchida et al. (1997) in their analysis of the CAM spectra of a number of reflection nebulae. Our models include continuum emission from PAHs only at $\lambda \gtrsim 15$ μm (see Fig. 3). Together with emission by large grains, they can roughly account for the continumm emission observed in the lw9 filter, but not for the continuum at shorter wavelengths, even when we allowed the size range of the very small grains to vary (see Natta et al. 1993 for a discussion of the dependence of very small grain emission on grain parameters). We suspect that the adopted continuum cross sections of transiently heated species are incorrect in the infrared. In fact, these and other ISO results could be used to better constrain the continuum cross section of these species.

4.4. Mass of Circumstellar Material

An interesting possibility opened up by our observations is to derive the mass of circumstellar material from the observed intensity of the PAH features.

We know the geometry of the emitting region, i.e., the approximate distance of the grains from the star. For a given distance and stellar luminosity, the integrated 6 to 14μm flux is directly proportional to the number of C atoms in PAHs. This is because the PAHs account for the total emission in this spectral region (Fig. 3). The fraction of C atoms in PAHs is known to within a factor of three, so we can directly convert the carbon column density $N_{\rm C}$ derived by fitting the feature intensities into a hydrogen column density $N_{\rm H}$. The uncertainty on $N_{\rm H}$ is probably comparable to the uncertainty that affects its determination from sub-millimeter continuum observations (see, for example, Krügel & Siebenmorgen, 1994). The mass of gas and dust can then be computed from the values of $N_{\rm H}$ averaged over the region of interest.

We derive a total mass of the circumstellar material in a region of about 0.03 pc radius (33″) of about 0.07M$_\odot$

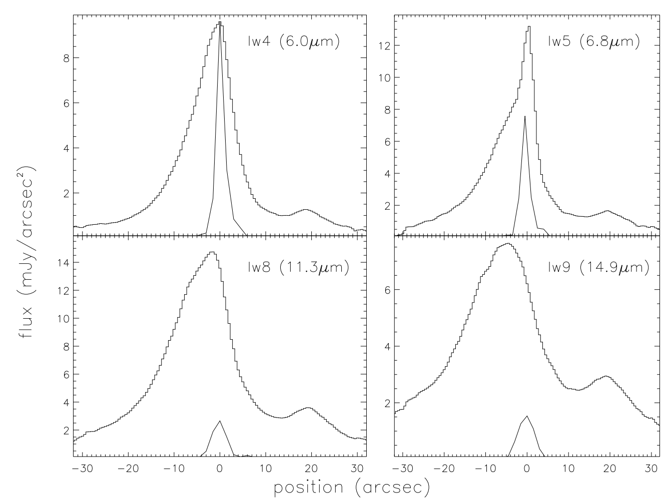

Fig. 4. Intensity as a function of the distance from the star along the direction indicated in Fig. 1 for the four narrow band filters lw4 (6.0 μm), lw5 (6.8 μm), lw8 (11.3 μm) and lw9 (14.9 μm). For comparison we show the point spread function for each filter normalized to the photospheric flux of the star and centered at the position of the star.

of which 0.03$M_\odot$ is in the elongated ring structure and only 0.003$M_\odot$ in the central region of ∼1600 AU radius. Our estimates agree with the upper limit $\lesssim$0.015 $M_\odot$ in a region of size 23″ (2000 AU radius) derived from the 1.3mm flux (< 91 mJy; Henning et al. 1993).

4.5. The Origin of the Ring

The ring structure is clearly seen in the enhancement of the column density in position 7 (see Table 2). It has a projected size of about 0.045×0.03 pc (50×36″), a thickness of about 0.01 pc and a mass of ∼0.03 $M_\odot$. Its density is of the order of 3×10^4 cm^{-3}.

The presence of PAHs in the ring indicates that it is made of interstellar matter, rather than of matter ejected from the star. Its morphology suggests that the ring structure has been created by the interaction of the star with the surrounding matter.

It is possible that the ring results from the interaction of a stellar wind with the environment. In this hypothesis, the material in the ring is swept-up gas. The ring coincides with the inner wall of a three-dimensional cavity created by the wind. If we take a ring radius ∼0.02 pc and an average ambient density $\sim 2 \times 10^4$ cm^{-3} (as derived from the column densities in position 8; see Table 2), the swept-up mass is ∼0.015$M_\odot$, comparable to the estimated ring mass. Since there is no evidence of a stellar wind at the present time, the ring formation must be due to an episode of mass-loss, which has died out very recently. Assuming that the ring is expanding at 5 km s^{-1} (there is no dynamical information available), we estimate the momentum in the ring to be $\sim 3 \times 10^{37}$ gr cm s^{-1}. If we take as a typical timescale the dynamical age of the ring expansion (4000 yr), we find that the ring momentum could have been provided by a wind episode characterized by velocity 350 km s^{-1}(Finkenzeller and Mundt 1984) and mass-loss rate $\sim 10^{-7}$ $M_\odot$ yr^{-1} typical of winds in Herbig Ae/Be stars (Nisini et al. 1995). Note that these estimates depend on our assumption of an expansion velocity for the ring, that would be very interesting to measure directly.

A second possibility is that the ring is due to the action of the radiation pressure from the star. The radiation pressure at the ring ($\sim L_\star/(4\pi$ c $R^2)$) is $\sim 10^{-10}$ erg cm^{-3}, comparable with the thermal pressure of the ambient medium $nkT \sim 1.4 \times 10^{-10}$, with $n \sim 2 \times 10^4$ cm^{-3} and $T \sim 50$K, the typical temperature of the large grains at the distance of the ring.

The ring is not centered on the star, which is closer to the NW edge than to the SE. This asymmetry may be related to a density gradient in the ambient medium, if the density is higher to the NW than to the SE. Since HD 97300 is very likely located near the front edge of the Chamalion I cloud, the best tracer of its immediate environment is an optically thick molecule such as ^{12}CO. The ^{12}CO map of Mattila et al. (1989) shows an enhancement of the radiation temperature just to the NW of HD 97300.

Finally, it is interesting that HD 97300 is not the only Herbig AeBe star with a ring. A similar structure (although about 3.5 times larger) is seen in scattered light in the younger and more deeply embedded star LkHα198 (Leinert et al. 1991). Also in that case the ring has an elliptical shape and the exciting star is shifted from its center. Both LkHα198 and HD 97300 have an embedded companion with projected separation much smaller than the size of the ring. It is possible that binarity plays a role in shaping the ring. In LkHα198, there is a CO outflow (Levreault 1988), roughly aligned with the reflection nebulosity, whose association to LkHα198 itself is, however, uncertain. We do not know if there is PAH emission associated with the LkHα198 ring.

5. Summary and Conclusions

We have presented in this paper mid-IR images and spectra of the pre-main–sequence star HD 97300 obtained with ISOCAM on board of ISO.

The images show extended emission, an elliptical ring structure of size about 0.045×0.03 pc, and two peaks of emission, separated by about 3″, displaced from the center of the ring in the NW direction. One of the two emission peaks is detected in the three filters at shorter wavelengths and coincides with the nominal position of the central star. The other peak is only visible in the two filters at longer wavelengths, and we suggest that it may be an embedded companion of HD 97300 similar to that seen in the 10μm images of Lagage et al. (1993) of the region around the younger Herbig AeBe star LkHα198.

The CVF data reveal that the emission in this region is dominated by the IEBs. We fit the spectra in selected positions at increasing distance from the star with a dust model which includes PAHs, very small particles and large grains. At the spectral resolving power of ISOCAM a simple classical oscillator model is sufficient to account for the strengths and shapes of the infrared emission bands. Transiently heated species (PAHs and possibly very small grains) very likely produce also the continuum emission, clearly detected in the range 9–11μmand 14–16 μm, with contribution by large grains only at the longest wavelengths.

The elliptical ring has a mass of about 0.03 $M_\odot$ (from the model fits to the IEB intensity) and surrounds an almost empty cavity. We believe that its origin may be due to the interaction of the visible star HD 97300 with the surrounding matter. Two possible mechanisms can account for its properties; either a past mass-loss episode with rate $\sim 2\times10^{-8}$ $M_\odot$ yr^{-1} and duration $\sim 5\times10^4$ yr, or radiation pressure. Both are consistent with the known properties of HD 97300. The off-center location of the star with respect to the ring may be the effect of a density gradient in the SE–NW direction in the outer region of the Chamalion I cloud where HD 97300 lies. The ring is reminiscent of the structure observed in scattered light around the Herbig Ae/Be star LkHα198.

Acknowledgements. We are indebted to François Boulanger for having shared with us prior to publication, his ideas on the profiles of PAH features. We thanks Mario van den Ancker and Malcolm Walmsley for interesting comments to this paper. This work was supported in part by CNR grant 97.00018.CT02 and ASI grant ARS-66-96 to the Osservatorio di Arcetri.

References

Abergel A.nrd J.P., Boulanger F. et al., 1996, A&A 315, L329
Allamandola L.J., Tielens A.G.G.M., Barker J.R., 1989, ApJ Suppl, 71, 733
Biviano A., Alteri B., Blommaert J., et al., 1997, in:Processings of the First ISO Workshop on Analytical Spectroscopy with SWS, LWS, PHT-S and CAM-CVF, A.M. Heras, K. Leech, N.R. Trams, M. Perry (eds.), Madrid, Spain, 6-8 October, 1997.
Blommaert J., 1997, ISOCAM Photometry report, *isowww.estec.esa.nl/instr/CAM/calwksp.*
Boulanger F., Reach W.T., Abergel A., et al., 1996, A&A 315, L325
Butner H.M., Natta A., 1995, ApJ 440, 874
Cesarsky C., Abergel A., Agnèse P. et al., 1996a, A&A 315, L32
Cesarsky D., Lequeux J., Abergel A. et al., 1996b, A&A 315, L305
Cesarsky D., Lequeux J., Abergel A. et al., 1996c, A&A 315, L309
Duley W.W., 1989, MNRAS 234, 61
Henning Th., Pfau W., Zinnecker H., Prusti T., 1993, A&A 276, 129
Finkenzeller U., Mundt R., 1984, A&AS 55, 109
Kessler M.F., Steinz J.A., Anderegg M.E. et al., 1996, A&A 315, L27
Krügel E., and Siebenmorgen R., 1994, A&A 288, 929
Lagage P.-O., Olofsson G., Cabrit S. et al., 1993, ApJ 417, L79
Leinert Ch., Haas M., Lenzen R., 1991, A&A 246, 180
Levreault R.M., 1988, ApJ 330, 897
Mattila K., Liljeström T., Toriseva M., 1989, in:*Low Mass Stars Formation and Pre-Main Sequence Objects*, B. Reipurth ed., ESO Workshop Proceedings n.33, p.153
Nisini B., Milillo A., Saraceno P., Vitali F., 1995, A&A 302, 169
Natta A., Prusti T., Krügel E., 1993, A&A 275, 527
Papoular R., Conard J., Guiliano M., Kister J., Mille G., 1989, A&A 217, 204
Prusti T., Natta A., Palla F., 1994, A&A 292, 593
Rydgren A.E., 1980, AJ 85, 444
Sakata A., Wada S., Tanabe T., Onaka T., 1984, ApJ 287, 151
Schutte W.A., Tielens A.G.G.M, Allamandola L.J., Cohen M., Wooden D.H., 1990, ApJ 360, 577
Schutte W.A., Tielens A.G.G.M, Allamandola L.J., 1993, ApJ 415, 397
Siebenmorgen R., Krügel E., 1992, A&A 259, 614
Siebenmorgen R., Krügel E., Mathis J.S., 1992, A&A 266, 501
Siebenmorgen R., Starck J.L., Cesarsky D.A., Guest S., Sauvage M., 1997, "ISOCAM Data Users Manual Version 3.0", ESA document, Reference: SAI/95-222/Dc, *isowww.estec.esa.nl/instr/CAM/.*
Starck J.L., Siebenmorgen R., Gredel R., 1997a, ApJ 482, 1011
Starck J.L., Bijaoui A., Murtagh F., 1997b, Image Processing and Data Analysis in the Physical Science: The Multiscale Approach, Cambridge University Press (in press).
The ISOCAM Team, 1996, ISOCAM Observer's Manual, *http : //isowww.vilspa.esa.es* : 1909*/manuals/isocam/*
Thé P.-S., Wesselius P.R., Tjin A Djie H.R.E., Steenman H., 1986, A&A 155, 347
Uchida K.I., Sellgren K., Werner M., 1997, ApJ 493, L109
van den Ancker M.E., Thé P.-S., Tjin A Djie H.R.E., et al., 1997, A&A 324, L33
Whittet D.C.B., Prusti T., Franco G.A.P., et al., 1997, A&A 327, 1194